

AIAA 97-2008

Feedback algorithms for turbulence control—some recent developments

Petros Koumoutsakos, Thomas R. Bewley, Edward P. Hammond, & Parviz Moin Center for Turbulence Research NASA Ames/Stanford University Stanford, California 94305-3030

28th AIAA Fluid Dynamics Conference 4th AIAA Shear Flow Control Conference

June 29 - July 2, 1997 Snowmass Village, CO

Feedback Algorithms for Turbulence Control— Some Recent Developments

Petros Koumoutsakos, Thomas R. Bewley, Edward P. Hammond, and Parviz Moin Center for Turbulence Research, NASA Ames/Stanford University, Stanford, California 94305

Abstract

Some recent developments on the feedback control of turbulent flows are presented. Physical mechanisms associated with opposition control algorithms are investigated. A new control method based on the sensing and manipulation of vorticity creation at the wall is presented. The results indicate that significant drag reduction can be achieved using wall information only. The potential for optimization of feedback control algorithms, using neurocomputing methodologies is outlined.

1 Introduction

The active feedback control of turbulence in engineering flows is gaining recognition as a possible means for greatly improved performance of aerospace and marine vehicles. While passive devices have been used effectively in the past, active control strategies have the potential of allowing a significant improvement in the performance of future configurations.

Along with small and robust sensors and actuators, simple yet effective control algorithms, which are based on measurable flow quantities, are needed to make active feedback control of turbulence a reality. In this paper we discuss two feedback algorithms for turbulence control: the opposition control scheme, introduced by Choi, Moin, & Kim (1994), and a novel feedback algorithm based on the manipulation of the wall vorticity flux, proposed by Koumoutsakos (1997).

In the opposition control approach, the vertical motion of the turbulent flow near the wall is countered by an opposing blowing/suction distribution of velocity on the wall. The effectiveness of the opposition control algorithm depends strongly on the location of sensing: a 25% drag reduction is observed when the wall normal velocity field is sensed at $y^+ \approx 15$ in a low Reynolds number turbulent channel flow, whereas a large increase in drag is observed when the sensing location is at $y^+ \approx 25$. One of the purposes of this paper is to investigate the mechanisms of this fundamentally different behavior.

Though the opposition control algorithm is simple and effective for viscous drag reduction, it has the substantial drawback that it requires measurements inside the flow domain. In order to alleviate this difficulty, Lee, et al. (1997) employed a neural network to construct a simple feedback control algorithm using infor-

mation only at the wall. Their methodology was shown to reduce skin friction by about 20%. We outline here an alternative novel feedback control algorithm based on information that can be obtained at the wall. This framework is based on the identification of the nearwall structures via their induced wall vorticity flux. The present control scheme is based on the manipulation of the spanwise and streamwise vorticity flux components, which can be obtained as a function of time by measuring the instantaneous pressure at the wall and calculating its gradient. An algorithm is presented which allows for the explicit calculations of the necessary control strengths. Application of the present control scheme to low Reynolds number turbulent channel flow produced drag reduction of up to 40% using wall information only.

The opposition and vorticity flux feedback control algorithms are based on physical mechanisms of vortex-wall interactions. Although they have been proven to be effective in reducing the skin friction drag in turbulent flow simulations, an optimization procedure is necessary to increase their effectiveness and their applicability to practical configurations. We outline the potential of neurocomputing methodologies (such as neural networks and evolutionary strategies) to achieve this optimization.

In §2 of this paper we analyze the opposition control algorithm. The framework of vorticity flux is outlined in §3 and the application of the method to two and three dimensional flows is reported in §4. An outline and some preliminary investigations of neurocomputing ideas for the optimization of feedback control algorithms is presented in §5. Recommendations for future work and conclusions are presented in §6.

2 Opposition control

Turbulent channel flows are dominated in the region within 50 viscous units from the walls by vortices which tend to be aligned nearly in the streamwise direction and slightly inclined to the wall. As they evolve, these vortices "pump" high momentum fluid from the core region of the channel towards the walls ("sweep events"), and low momentum fluid from the near-wall region towards the center of the channel ("ejection events"), creating local regions of high and low shear at the walls ("streaks"). The resultant mixing of the high- and low-momentum fluid in the channel results in a fuller mean velocity profile and much higher viscous drag than that of a laminar flow at the same bulk velocity.

Published by the American Institute of Aeronautics and Astronautics, Inc. with permission.

As first investigated by Choi, Moin, & Kim (1994) and shown in figure 1, the idea of opposition control is simply to counter the vertical velocity near the wall with an opposing control velocity at the wall in order to reduce this mixing. When opposing the vertical motion at $y^+ \approx 15$, the con-

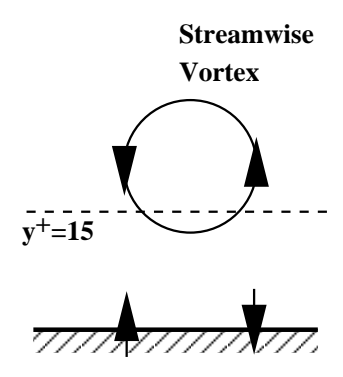


Figure 1: Opposition control.

trol is found to do much more than simply inhibit the formation of the streaks—it actually mitigates the process of the turbulence production itself. This results in much lower turbulence levels and approximately 25% drag reduction (figure 2). When the control is set more ambitiously to counter motions farther from the wall, at $y^+ \approx 25$, the drag soon climbs to very high levels. Note that present results indicate detection at $y^+ = 15$, a case not tested by Choi, Moin, & Kim (1994), is slightly more effective than detection at $y^+ = 10$.

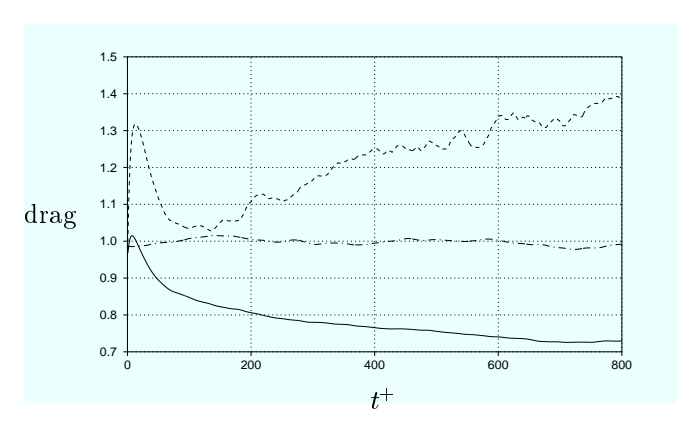


Figure 2: Evolution of drag at $Re_{\tau} = 180$. Solid, detection at $y^+ = 15$; dot-dashed, no control; dashed, detection at $y^+ = 25$. Drag is normalized by its average uncontrolled value.

Three high-resolution computations were performed, as described in figure 2, at $Re_{\tau}=180$. (Re_{τ} is the Reynolds number based on the shear velocity of the uncontrolled flow and the channel half-width; the corresponding Reynolds number based on centerline velocity is $Re_c=3300$.) These computations used a hybrid code (Bewley 1997) that is spectral in the streamwise direction x and spanwise direction z and second order finite difference in the wall-normal direction y. (Note: u, v, and w correspond to the velocities in the x, y, and z directions respectively.) A staggered grid of $256 \times 128 \times 256$ mesh points was used. A third-order Runge-Kutta algorithm was used for time advancement.

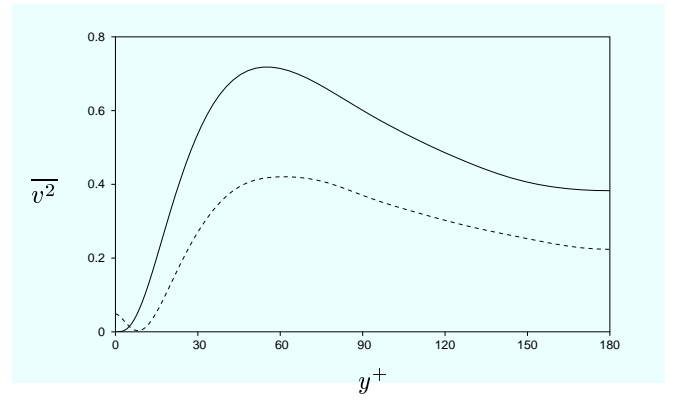


Figure 3: Time averaged $\overline{v^2}$ across the channel half width: solid, no control; dashed, detection at $y^+ = 15$. Note the formation of a plane of zero vertical velocity.

As shown in figure 3, the control scheme with detection at $y^+=15$ creates a "virtual wall" in the fluid halfway between the physical wall and the detection plane. The reduced mixing of the core fluid with the near-wall fluid due to this virtual wall significantly reduces the overall turbulent energy, as shown by comparison of figures 5a and 6a. Convective transport of momentum no longer occurs across the plane of the virtual wall. The only mechanism for transport of momentum in the wall-normal direction in this case, then, is diffusion by viscosity, which is relatively less effective than convective transport.

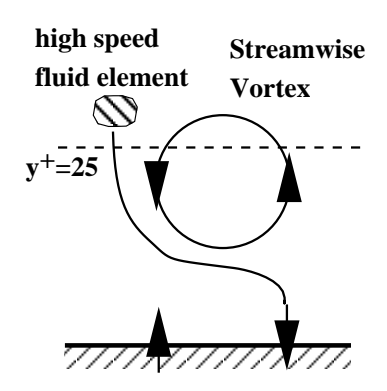
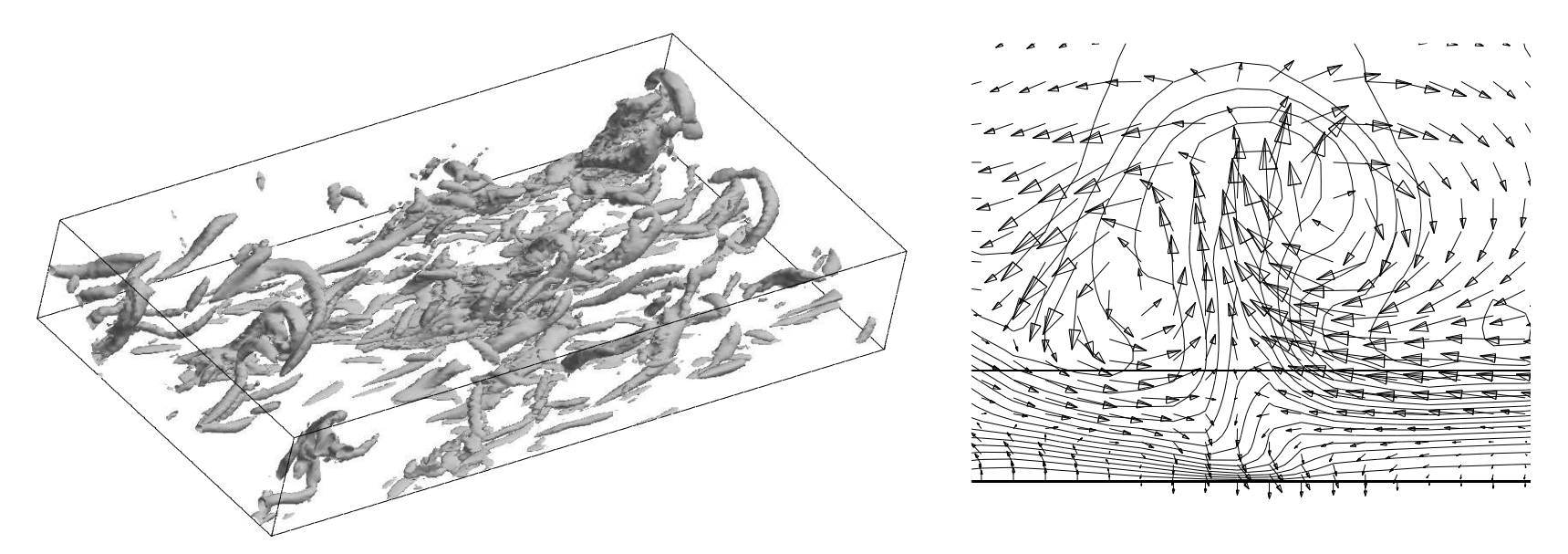


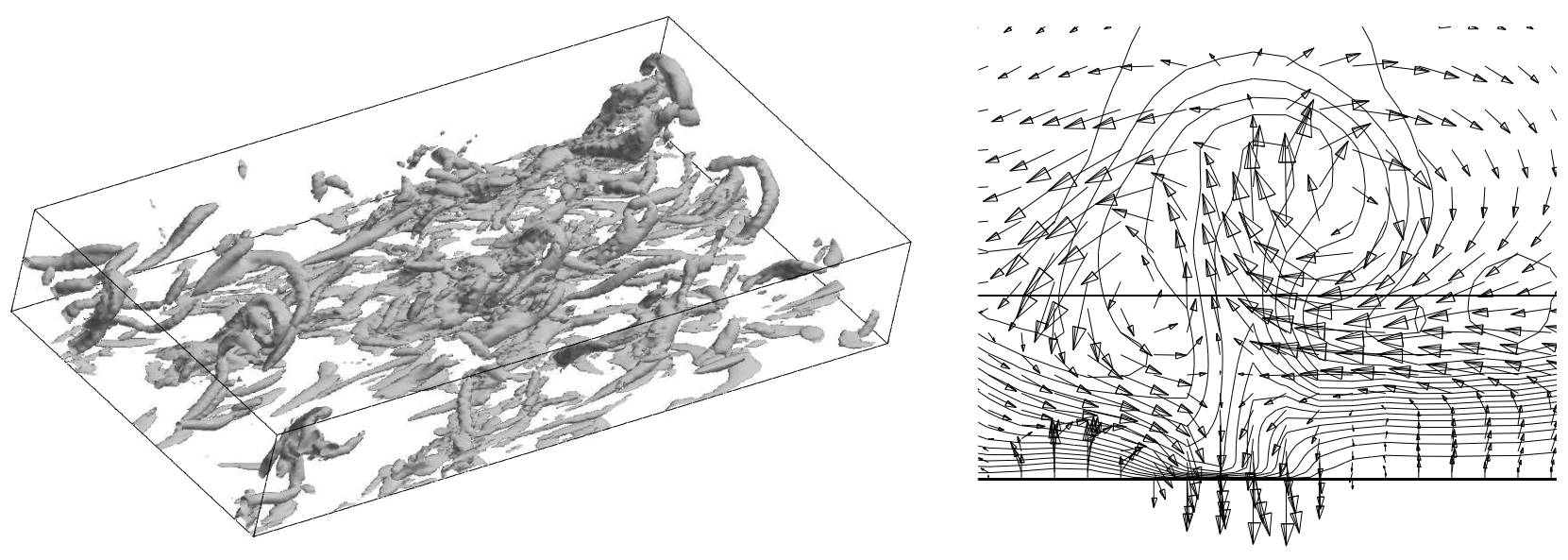
Figure 4: Skewed path by which sweep event is attracted towards wall for detection at $y^+ \geq 25$.

The controller with detection at $y^+ = 25$ resulted in the channel eventually filling with turbulent fluctuations, as shown in the oblique view of figure 6b. As the control was turned on, certain flow conditions would consistently act to destabilize the flow. This result is well explained by analysis of the flow situation shown in the cross-flow plane of figure 5b and schematically in figure 4. It was observed that the

controlled system developed skewed paths by which high speed fluid from nearby sweep events could be drawn towards the wall below an ejection event, as shown in figure 4. The detection plane is too far from the wall to accurately reflect the influence of the flow structures nearest to the wall. In this case, the "virtual wall" is not established, resulting in increased turbulent activity and mixing in the near-wall region.

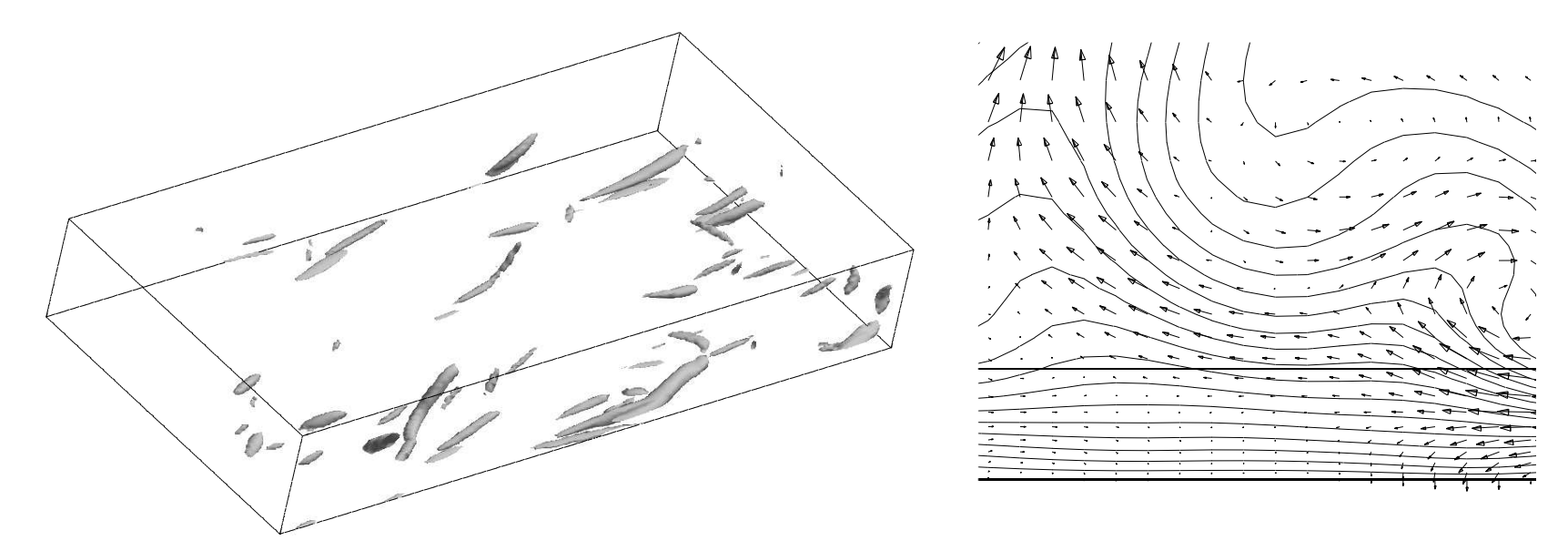


(a) Opposition control with detection at $y^+ = 15$ (drag-reducing case). Small control velocities at wall (heavy horizontal line) create a plane midway between wall and detection plane (thin horizontal line) with almost zero vertical velocity, effectively insulating the wall from high-drag sweep events.

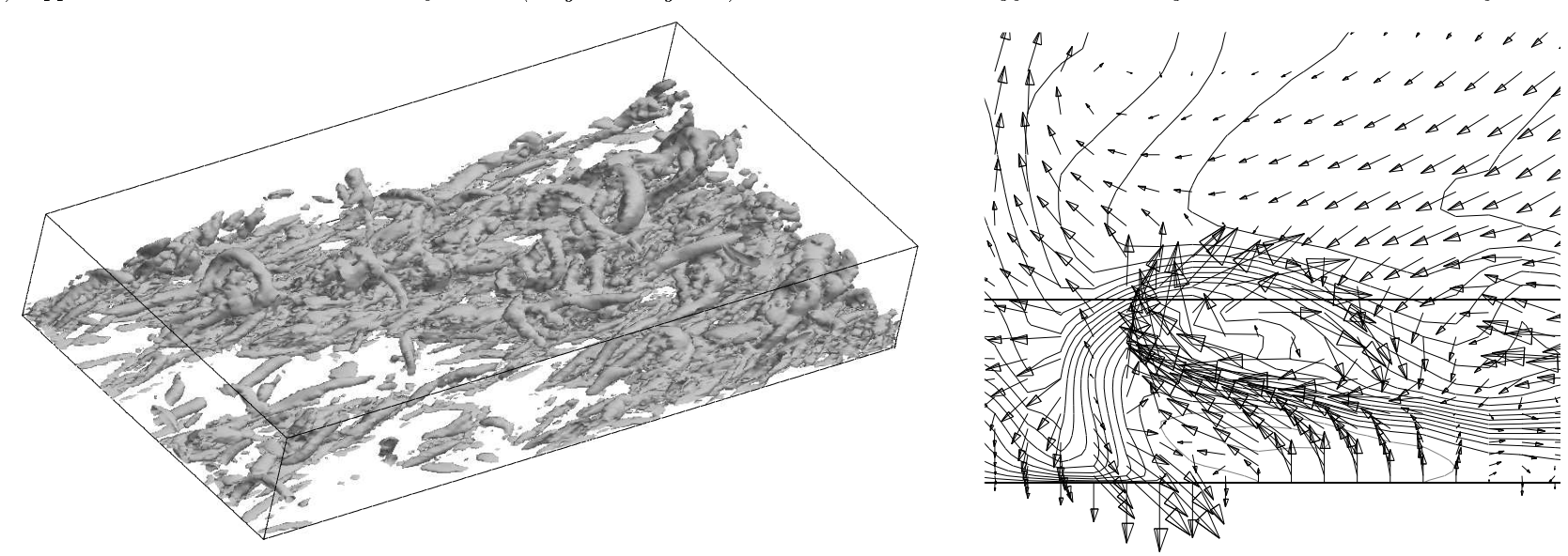


(b) Opposition control with detection at $y^+ = 25$ (drag-increasing case). Larger control velocities, responding to flow fluctuations farther from wall, sometimes create a skewed path by which high speed fluid from a nearby sweep event may be drawn towards the wall below an ejection event.

Figure 5: Drag-reducing/increasing control cases at $t^+=9$, a short time after control is applied. Note that free stream flow structures are almost identical, yet the control response in (b) is much stronger. Oblique view: isosurfaces of discriminant of velocity gradient tensor; one quarter of lower half of computational domain shown. Cross-flow plane: cross-flow velocity vectors and streamwise velocity contours.



(a) Opposition control with detection at $y^+ = 15$ (drag-reducing case). Turbulent kinetic energy and total drag have decreased substantially.



(b) Opposition control with detection at $y^+ = 25$ (drag-increasing case). Mechanism described in figure 5b persists and proves to be unstable, resulting in highly enhanced levels of turbulence and increased drag.

Figure 6: Drag-reducing/increasing control cases at $t^+ = 279$, a long time after control is applied. Discriminant isosurface value, cross-flow velocity vector scale, and streamwise velocity contour values identical to those in figure 5.

3 Vorticity flux control— Outline

Although the velocity opposition control scheme was successful in reducing the skin friction drag, it is not readily suitable for practical implementation as it relies on off-wall information. Choi, Moin, & Kim (1994) examined the relationship between variables available at the wall (such as pressure, shear stresses, etc) and the flow above the wall. An opposition control scheme using a quantity derived from the Taylor series expansion of the normal velocity component about the wall, resulted in a 6% drag reduction. Recently, Lee, et al. (1997) implemented a neural network to approximate the correlation between the wall shear stresses and the wall actuations. A simple control network employing this technique reduced the skin friction drag in a turbulent channel flow by 20%, using wall information only.

We outline in this section the development of a novel feedback control algorithm (Koumoutsakos, 1997) based on the manipulation of the vorticity creation at a wall, using wall information only. The pressure field is sensed at the wall and its gradient (the wall vorticity flux) is calculated. Blowing/suction at the wall is the actuating mechanism and its strength is calculated explicitly by formulating the mechanism of vorticity generation at a no-slip wall.

3.1 Formulation

In wall bounded flows, the tangential motion of fluid elements relative to the wall establishes velocity gradients. With the definition of vorticity (ω) as the curl of velocity ($\omega = \nabla \times \mathbf{u}$), this may be equivalently described in terms of the vorticity that is acquired by the fluid elements near the wall. Lighthill (1963) envisioned the wall as a system of sources and sinks of vorticity.

A measure of the vorticity that enters the flow is given by the wall normal vorticity flux. The equation for the evolution of the vorticity field at the wall degenerates into a diffusion type equation:

$$\frac{\partial \boldsymbol{\omega}}{\partial t}|_{\mathbf{w}} = -\nabla \cdot (-\nu \nabla \boldsymbol{\omega})|_{\mathbf{w}} \tag{1}$$

where ν is the kinematic viscosity of the fluid and the subscript w denotes quantities measured at the wall. The fluid elements adjacent to the wall acquire vorticity according to the source term defined by the wall vorticity flux tensor (Hornung 1990) $J_w = -\nu \nabla \omega$. We are interested in the vorticity acquired by the fluid elements near the wall, and hence the wall normal component of this source tensor, defined as the wall vorticity flux vector $\sigma = \mathbf{n} \cdot J_w$.

For simplicity, in the rest of this paper we consider a cartesian coordinate system and flow over a flat wall identified with the xz plane, normal to the y-axis. The

vorticity flux is then expressed as:

$$\sigma = -\left(\nu \frac{\partial \omega}{\partial y}\right)_{w}$$

For an incompressible viscous flow over a stationary wall, the vorticity flux is directly proportional to the pressure gradients, as the momentum equations reduce at the wall to (Panton 1984):

$$\nu \left(\frac{\partial \omega_{x}}{\partial y} \right)_{w} = \frac{1}{\rho} \left(\frac{\partial P}{\partial z} \right)_{w}, \quad -\nu \left(\frac{\partial \omega_{z}}{\partial y} \right)_{w} = \frac{1}{\rho} \left(\frac{\partial P}{\partial x} \right)_{w}$$

where P is the pressure and $\omega_{\rm x}$ and $\omega_{\rm z}$ are the streamwise and spanwise vorticity components. Note that the flux of the wall normal vorticity, $\omega_{\rm y}$, may be determined from the kinematic condition $(\nabla \cdot \boldsymbol{\omega} = 0)$.

3.2 Measurements of the wall vorticity flux

Experimental measurements of the wall vorticity flux in a turbulent flow have been reported by Andreopoulos & Agui (1996). They used high frequency response transducers to measure fluctuating wall pressure gradients and then compute the vorticity flux in a two-dimensional turbulent boundary layer. Their measurements demonstrated the significance of vorticity flux in describing near wall processes. They made an attempt to correlate vorticity flux signals with physical phenomena such as bursting-sweep processes in the boundary layer. They observed that fluid acquires or loses vorticity at the wall during rather violent events followed by periods of small fluctuations. Their experiments demonstrated that the major contributions to the vorticity flux come from the uncorrelated part of the pressure signals, at two adjacent locations, which contain a wide range of vortical scales. As the degree of correlation is smaller between the small scales their contribution to the vorticity flux is more pronounced. This imposes a severe requirement on the spatial resolution of the pressure gradients/vorticity flux measurements. Practical applications (Moin & Bewley 1995) would require actuators and sensors with sizes in the order of $50\mu m$ and actuator frequencies of 1MHz. Recent advances in micro pressure sensor fabrication technology (Ho & Tai 1996) give us an opportunity to overcome these difficulties. Löfdahl, Kälvesten, & Stemme 1996 presented measurements in a two-dimensional flat plate boundary layer with a resolution of eddies with wave numbers less than ten viscous units using microscopic silicon pressure transducers. It appears that using this new technology one may be able to describe in detail physical processes in terms of the wall vorticity and the wall vorticity flux.

3.3 Vorticity flux induced by blowing and suction at the wall.

The role of the vorticity flux from oscillating walls as a mechanism for the control of unsteady separated flows was discussed by Wu, Wu, & Wu (1993). They concluded that wall oscillations can produce a mean vorticity flux that is partially responsible for phenomena of vortex flow control by waves. Gad-El-Hak (1990) has shown that the vorticity flux can be affected by wall transpiration as well as by wall-normal variation of the kinematic viscosity (ν) as a result of surface heating, film boiling, cavitation, sublimation, chemical reaction, wall injection of higher/lower viscosity fluid, or in the presence of shear thinning/thickening additive.

However these works do not provide us with an explicit formulation for the actuator strength necessary to induce a desired vorticity flux at the wall. This may be achieved by considering the generation of vorticity at the wall as a fractional step algorithm (Lighthill 1963). At each time step (δt) the no-slip boundary condition can be rendered equivalent to a vorticity flux boundary condition (Koumoutsakos, Leonard, & Pepin 1994) which is materialized in successive substeps. During the first substep we consider the inviscid evolution of the vorticity field in the presence of solid boundaries. The no-through flow boundary condition is enforced, via the introduction of a vortex sheet $\gamma(s)$ along the surface (s) of the body. The vortex sheet is equivalent to a spurious slip velocity on the boundary that needs to be eliminated in order to enforce the no-slip boundary condition. This is achieved at the next substep of the algorithm, as the vortex sheet enters diffusively into the flow field. When γ is eliminated from the body surface in the interval $[t, t + \delta t]$ the circulation (Γ) of the flow field would be modified according to:

$$\oint \gamma(s) \, ds = \int_{t}^{t+\delta t} \frac{\mathrm{d}\Gamma}{\mathrm{d}t'} \, dt' \tag{2}$$

On the other hand Kelvin's theorem states that the rate of change of circulation induced to the fluid elements due to the presence of the body is:

$$\frac{\mathrm{d}\Gamma}{\mathrm{d}t} = \nu \oint \frac{\partial \omega}{\partial n}(s) \, ds \tag{3}$$

If we consider this vorticity flux to be constant over the small interval of time (δt) , we will have:

$$\nu \frac{\partial \omega}{\partial n}(s) = -\gamma(s)/\delta t \tag{4}$$

This constitutes then a Neumann type vorticity boundary condition for the vorticity field equivalent to the no-slip boundary condition (Koumoutsakos, Leonard, & Pepin 1994).

This formulation helps us determine the vorticity flux induced by a set of actuators, such as ideal sources/sinks located at the wall. Without loss of generality we consider a two-dimensional flow over a flat wall, and a system of sources/sinks of strength q_i that are distributed

uniformly over a panel of size d_j , centered at locations x'_j , j=1,2,3,...N. When the sources/sinks are switched on the induced tangential velocity at point x_i on the wall and the corresponding vorticity flux can be determined as:

$$\nu \, \delta t \, \frac{\partial \boldsymbol{\omega}}{\partial y}(x_i) = \sum_{j=1}^{N} \frac{q_j}{2\pi} \, \int_{-d_j/2}^{d_j/2} \frac{ds}{x-s}$$
 (5)

where $x = x_i - x'_j$. The methodology outlined herein may be formulated for a variety of actuators, such as wall acceleration, deformation, etc.

3.4 An active control strategy.

For the purposes of our control scheme we consider a series of vorticity flux (or equivalently pressure gradient) sensors on the wall at locations $x_i, i=1,2,3,...M$. Using the formulas described above we can explicitly determine the actuator strengths necessary to achieve a desired vorticity flux profile at the wall at a time instant, k, by solving the linear set of equations:

$$Bu_k + X_{k-1} = D_k \tag{6}$$

where $D_k = (\frac{\partial \omega^k}{\partial y}(x_1), \frac{\partial \omega^k}{\partial y}(x_2), ..., \frac{\partial \omega^k}{\partial y}(x_M))$ is an $M \times 1$ vector of the desired vorticity flux at the sensor locations, $X_{k-1} = (\frac{\partial \omega^{k-1}}{\partial y}(x_1), \frac{\partial \omega^{k-1}}{\partial y}(x_2), ..., \frac{\partial \omega^{k-1}}{\partial y}(x_M))$ is an $M \times 1$ vector of the measured vorticity flux at the sensor locations and $u_k = (q_1^k(x_1'), q_2^k(x_2'), ..., q_N^k(x_N'))$ is an $N \times 1$ vector of source strengths at the actuator locations, B is an $M \times N$ matrix whose elements B_{ij} are determined by evaluating the integrals in Eq.5. The unknown source/sink strengths are determined by solving the system in Eq.6. If the relative locations of the sensors and actuators remain constant, matrix B need be inverted only once thus minimizing the computational cost of the method. For very large numbers of sensors and actuators, iterative methods along with multipole expansions may be implemented in order to further reduce the computational cost.

The present technique gives us the flexibility to adapt the actuator strengths to specific constraints. Practical considerations may constrain the control to jet-like actuators, $q_j \geq 0, j = 1, ..., N$ or to a blowing and suction configuration with a net zero mass flux;

$$\sum_{j=1}^{N} q_j = 0 \tag{7}$$

Such constraints may be easily incorporated in the above scheme by appropriately adjusting matrix B. A square, invertible matrix is always possible by accordingly modifying the number of sensors and actuators.

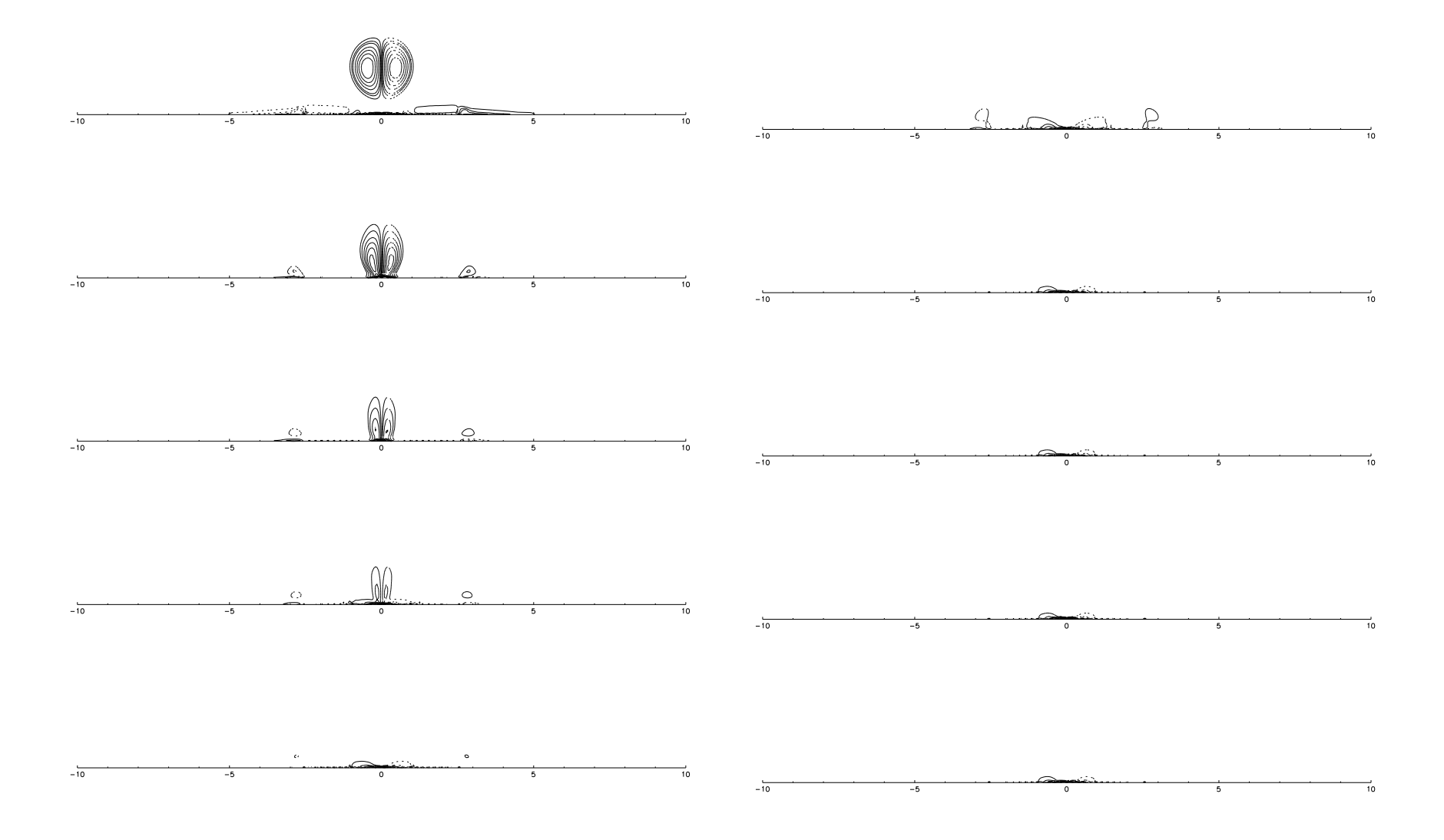


Figure 7: Vorticity contours of vortex dipole-wall interactions. Control canceling the wall vorticity flux.

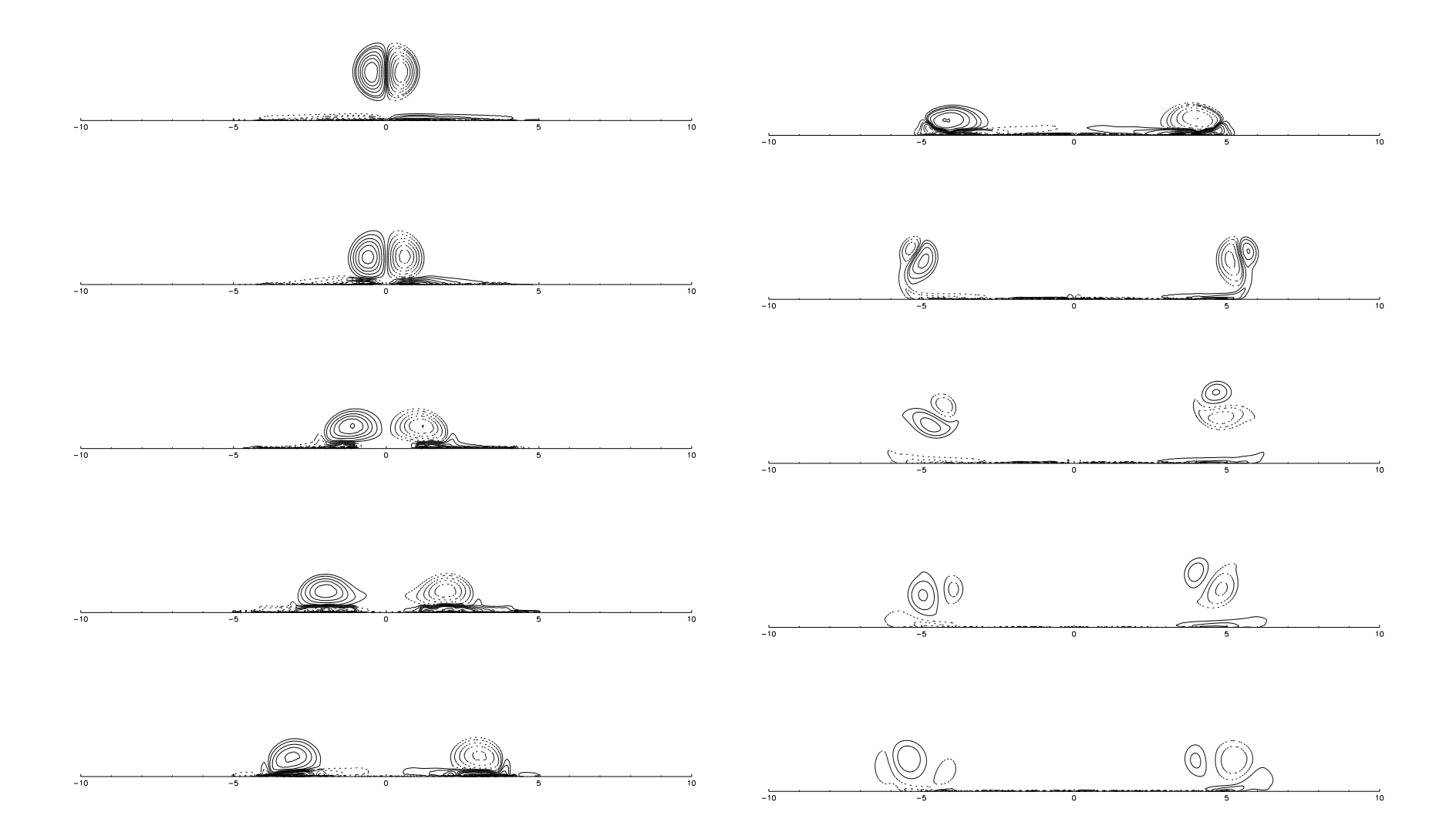


Figure 8: Vorticity contours of vortex dipole-wall interactions. Control enhancing the wall vorticity flux.

The simplicity of the present scheme allows for a number of different placements of sensors and actuators. Moreover, it allows for the *active* selection of the optimal locations (eg. for drag reduction) by suitable optimization algorithms. Here we chose the locations of sensors and actuators to be collocated. Physically this may be understood as an advantageous situation as the sensors are able to detect the vorticity field induced by the actuators which allows the control scheme to suitably compensate for it.

4 Vorticity flux control–Results

We present here preliminary results of the application of the proposed control scheme for two and three dimensional flows. In two dimensions we consider the model problem of a vortex dipole impinging on a wall, while in three dimensions low Reynolds number turbulent channel flow is considered. In both cases zero net mass transpiration is utilized to manipulate the vorticity flux induced by the flow at the wall.

4.1 Vortex dipole - Wall interaction

A Lamb's vortex dipole is considered impinging at the wall. The details of the initial vorticity configuration along with the employed high resolution viscous vortex method and simulations of the uncontrolled flow are detailed in Koumoutsakos (1997).

4.1.1 Canceling the wall vorticity flux

In this type of control we attempt to eliminate the vorticity flux at the sensor locations (i.e. set $D_k = 0$ in 6). The vorticity flux is measured at each instant and at the following time step we appropriately adjust the strength of the actuators by solving

$$B u_k = -X_{k-1} \tag{8}$$

for u_k . This scheme may be viewed as an *out-of-phase* control of the vorticity flux.

In figure 7 we present contour plots of the vorticity field of the controlled interaction of a vortex dipole with a wall. As the vortex descends towards the wall, the control scheme acts to eliminate the secondary vorticity generated at the wall. In turn, the primary vortex dipole 'sees' a permeable wall. At time T=1.0 the primary vortex dipole has been drawn into the wall.

A closer inspection of the vorticity field near the wall shows that the system of sensors and actuators reacts to the vorticity field generated by itself. An oscillatory set of small dipolar vortical structures is established near the wall and is sustained by the control algorithm.

4.1.2 Enhancing the wall vorticity flux.

In this case we attempt to enhance the generation of secondary vorticity at the wall. To achieve this, we require that the actuator strengths are adjusted so as to maintain the sensed vorticity flux (or equivalently $D_k = 2 X_{k-1}$ in 6) via the solution of the system:

$$B \vec{u}_k = \vec{X}_{k-1} \tag{9}$$

This scheme may be viewed as an *in-phase* control of the vorticity flux.

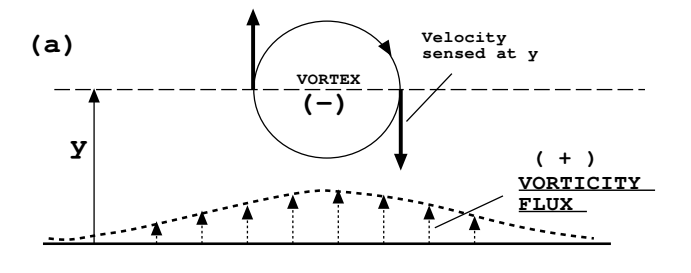
In figure 8 we present contour plots of the vorticity field. A system of sensors and actuators is distributed over a portion of the wall. As the vortex dipole approaches the wall it interacts with secondary vorticity. The control scheme acts to enhance the secondary vorticity, thus preventing the lift-off observed in uncontrolled vortex-wall interactions (Orlandi, 1990). The primary vortex components roll on the sheet of secondary vorticity that the actuators try to maintain. Lift off is prevented on the controlled portion of the wall, as the primary vortex components 'surf' the controlled portion of the wall. The vortical structures eventually lift-off outside the controlled region, as the primary vortices have not lost enough of their strength via diffusion.

4.2 Vorticity flux and opposition control

We remark here the relationship of the present active control strategy and the opposition control, discussed by Choi, Moin, & Kim (1994). In their simulations of control of a vortex dipole impinging at a wall the flow velocity normal to the wall is sensed at a distance off the wall. Blowing/suction is adjusted so as to oppose this velocity. As the primary vortex descends towards the wall, the blowing/suction counteracts this motion, enhancing the generation of secondary vorticity. This secondary vorticity in turn pairs-off with the primary vortex resulting in a vortex dipole propagating parallel to the wall. Clearly then one may observe that the opposition control scheme would produce different results depending on the location of sensing the wall normal velocity. Opposing the small wall normal velocity near the dipole center would prevent liftoff. On the other hand, opposing for example the velocity field farther away from the wall could result in destruction of the newly formed vortex dipoles.

The behavior of the vortex-wall interactions is strikingly similar to the vorticity field presented herein (compare figure 8 with figure 22b of Choi, Moin, & Kim (1994)) over the controlled part of the wall. This strongly suggests that the opposition control strategy and the vorticity flux control, are analogous. The two schemes differ in the way in which they sense the vorticity field that is near the wall and adjust the necessary blowing/suction at the wall. As shown in figure 9, counteracting the velocity field of the primary

vortex is equivalent to enhancing the generation of secondary vorticity, via the vorticity field generated by the set of sources and sinks. Although the two control schemes presented in this paper rely on two different descriptions of the vortex/wall interactions, they induce the same behavior to the vortical structures. As the vorticity flux control strategy relies on the sensing of the wall pressure and the calculation of its gradients, it appears as a promising method for practical applications. The analogy of the two schemes suggests that the successful results that have been obtained using the opposition control scheme could be obtained as well by the present strategy, using wall information only.



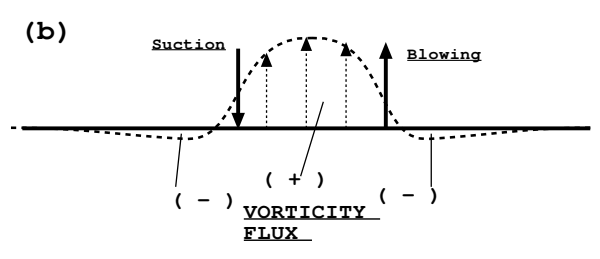


Figure 9: Vorticity flux generated by the opposition control algorithm.

4.3 Turbulent Channel Flow

We consider the application of the vorticity-flux control scheme on a low Reynolds number turbulent channel flow $(Re_{\tau}=200)$. The numerical method (Le, Moin and Kim 1997) is a fractional step algorithm in primitive variables $(\mathbf{u}-P)$, using central finite differences for spatial discretization and a third order Runge-Kutta time advancement scheme. Simulations were carried out with a grid resolution of $N_x \times N_z \times N_y = 128 \times 64 \times 128$. A cosine spacing was employed for the grid points in the wall-normal direction. The non-dimensional discretization is: $\Delta x^+ \approx 12$, $\Delta z^+ \approx 8$, $\Delta y^+ \approx 0.1 - 7$. A collocated arrangement of sensors and actuators was considered. In this arrangement the rows of sensors and actuators are located at alternating streamwise grid locations on the bottom wall. Their strength is determined using a technique similar to the two-dimensional techniques already described.

In the present scheme for three dimensional flows the 'desired' and the measured vorticity flux may be related by the following form:

$$\begin{pmatrix}
\nu \frac{\partial \omega_x}{\partial y} \\
\nu \frac{\partial \omega_z}{\partial y}
\end{pmatrix}_{control} = \begin{pmatrix}
a & b \\
c & d
\end{pmatrix} \begin{pmatrix}
\nu \frac{\partial \omega_x}{\partial y} \\
\nu \frac{\partial \omega_z}{\partial y}
\end{pmatrix}_{measured} (10)$$

The coefficients a, b, c, d may be chosen a-priori and they may be constant or spatially varying. The parameter space can be optimized for drag reduction/increase.

We have conducted several sets of simulations, varying locally and globally the coefficients a,b,c,d. Most of our simulations have been conducted with the set of parameters a=b=c=0 and $d=\pm 1$, which is equivalent to considering In/Out of phase control of the spanwise vorticity flux.

In figure 10 we present the drag coefficient for the uncontrolled and the controlled turbulent channel flow. These results indicate a drag decrease of up to 40% using out-of-phase control of the spanwise vorticity flux, using wall information only.

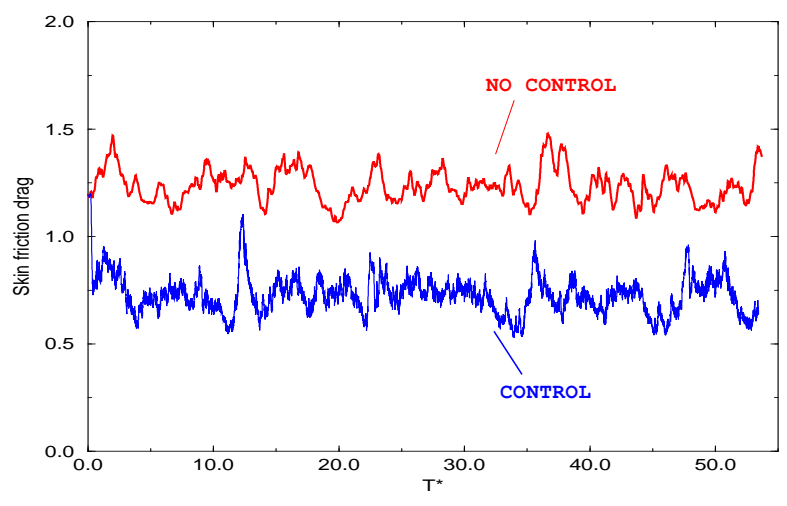


Figure 10: Vorticity flux control. Evolution of skin friction drag coefficient at $Re_{\tau}=200$.

5 Neurocomputing ideas for the optimization of feedback control algorithms

The feedback control algorithms, of opposition and vorticity flux control, are based on physical arguments. Although the results demonstrate the potential of these approaches, there is a clear need for further optimization. We are investigating the applicability of neurocomputing methodologies (e.g. evolution strategies, genetic algorithms, neural networks) for the optimization of different aspects of the feedback control algorithms.

The feedback control algorithms involve a large parameter space (actuator/sensor locations, strengths, time delay, phasing, etc.) that prevents the use of an exhaustive search for optimal configurations. Moreover, the possibility of applying these feedback control methodologies to realistic sensor/actuator configurations presents the challenge of a-priori unknown functional relationships between flow quantities (e.g. pressure, shear stresses) and actuator parameters. This eliminates the use of traditional optimization techniques and points in the direction of experimental optimization (Schwefel 1977). A systematic approach to experimental optimization problems, mimicking biological processes, has led to the development of evolution strategies (ES) and genetic algorithms (GA).

We are currently investigating evolution strategies to further optimize the wall vorticity flux feedback control algorithm. In particular, we examine the set, \mathbf{x} , of influence coefficients ($\mathbf{x} = [a,b,c,d]$) employed in Eq.10, whose relationship with the skin friction drag is not explicitly available. We conduct simulations of a turbulent channel flow, using a simple two member evolution strategy (Rechenberg 1973), to identify the coefficients in Eq.10 that led to drag minimization. A set of parameters is randomly initialized and is varied at certain time intervals according to :

$$\mathbf{x}^{n+1} = \mathbf{x}^n + N(0, \epsilon) \tag{11}$$

where $N(0,\epsilon)$ is a vector of independent random Gaussian numbers with zero mean and standard deviation ϵ . At the end of each interval the running average drag coefficient is examined and a new set of parameters is selected according to 11 when no drag decrease is observed.

In our preliminary investigations we considered variation of one or two member sets (for example $\mathbf{x} = [0,0,0,d]$ or $\mathbf{x} = [0,b,c,0]$). Our simple evolution strategies were not always able to converge to a set of parameters that leads to drag minimization. Nevertheless, the ES converged to the set [0,0,0,-1] that as was discussed in Section 4.3 results in drag minimization. Moreover the ES revealed a set of parameters that lead to drag minimization involving cross-coupling of the measured and

controlled streamwise and spanwise vorticity flux. (i.e. [a,b,c,d]=[0,-1,0,0]).

A related issue is the optimal placement of sensors and actuators. In the present simulations, the sensors and actuators coincide with the grid points on the wall. Hence, the non-dimensional streamwise spacing between the rows of sensor and actuators is $\Delta x^+ \approx 12$, whereas, the spanwise spacing is $\Delta z^+ \approx 8$. A parametric investigation is under way to determine the minimum spacing requirements for the sensor and actuator configurations. Although the number of possible configurations can be reduced using physical arguments, optimization techniques such as ES or GA's appear as suitable candidates.

Another issue is the time delay between the sensor and actuator signals in the vorticity flux control algorithm. The proposed methodology relies on measurements of the wall vorticity flux at one time step and the immediate adjustment of the actuator strengths at the following time step to achieve a desired vorticity flux. This can lead to systems that are not possible to realize experimentally. This process may be improved by identifying and appropriately manipulating, the time correlation of the vorticity flux signals at the sensor locations: $X_{k+1} = F(X_k, k)$ where $F(\cdot)$ is a nonlinear map The problem is then reduced to the identification of $F(\cdot)$, between the time instances $t = k\delta t$ and $t = (k+1)\delta t$. System identification techniques, involving another component of neurocomputing (neural networks) are presently under investigation. This procedure would be valuable also for practical applications, as it could provide the generally unknown correlations of realistic sensor/actuator parameters with quantities such as the wall vorticity flux. On a related front, as it was mentioned above, Lee, et al. (1997) have implemented neural networks, to eliminate the need of the opposition control algorithm for off-wall information. A neural net algorithm has been successfully employed, resulting in a 20% drag reduction for turbulent channel flow using wall information only.

In summary, neurocomputing algorithms (such as evolution strategies and neural networks), provide a valuable optimization tool, well suited to problems encountered by feedback control algorithms. Moreover, these methodologies have the potential to facilitate the implementation of active feedback control strategies to realistic configurations.

6 Conclusions

In this paper we discussed some recent research efforts to elucidate the physical mechanisms associated with the opposition control algorithm and to devise a new feedback control algorithm using wall information only. The optimization of feedback control algorithms using neurocomputing methodologies is outlined.

An extensive set of visualizations of direct numerical simulations of the opposition control, introduced by Choi, Moin, & Kim (1994), helped us elucidate its driving physical mechanisms.

A new feedback control algorithm (Koumoutsakos, 1997) based on the manipulation of vorticity creation at the wall was outlined. In this scheme the vorticity flux is sensed at the wall, via the measurement of wall pressure. A simple control strategy allows calculation of the strength of wall transpiration to achieve a desired wall vorticity flux. Using information available at the wall, the present control scheme is able to reproduce phenomena that were previously obtained computationally using off-wall information. Implementation of the vorticity flux feedback control algorithm in the simulation of a low Reynolds number turbulent channel flow, indicate unprecedented skin friction drag reduction ($\approx 40\%$)

using wall information only. Work is underway to implement the proposed strategy in the control of unsteady separated bluff body flows.

Neurocomputing methodologies, such as neural networks and evolution strategies, were investigated for the optimization of the feedback control algorithms. The results of Lee, et al. (1997) in the implementation of neural networks for the opposition control algorithm, and our preliminary investigations in the use of evolution strategies for the control of vorticity flux, suggest that such methodologies can be viable alternatives.

Acknowledgments

The authors gratefully acknowledge the funding provided by the AFOSR and the computer time provided by NASA-Ames Research Center in support of this project.

REFERENCES

Andreopoulos, J. & Agui, J.H. 1996 Wall-vorticity flux dynamics in a two-dimensional turbulent boundary layer. J. Fluid Mech. 309, 45-84.

Bewley, T.R. 1997 Optimal and robust control and estimation of transition and turbulence. Ph.D. dissertation, Stanford University.

Choi, H., Moin, P., & Kim, J. 1994 Active turbulence control for drag reduction in wall-bounded flows. J. Fluid Mech. 262, 75-110.

GAD-EL-HAK, M. 1990 Control of Low-Speed Airfoil Aerodynamics. AIAA J.118, 1537-1552.

Ho, C. & Tai, Y. 1996 Review: MEMS and its applications for flow control. J. of Fluids Engin. 118, 437-447.

HORNUNG, H. 1990 Sources of Vorticity. Ae 232. Class Notes, California Institute of Technology.

Johansson, A.V., Alfredsson, P.H., & Haritonidis, J.H. 1987 Evolution and dynamics of shear-layer structures in near-wall turbulence. J. Fluid Mech. 224, 579.

KIM, J., MOIN, P., & MOSER, R. 1987 Turbulence statistics in fully developed channel flow at low Reynolds number. J. Fluid Mech. 177, 133-166.

Koumoutsakos, P. 1997 Active Control of Vortex-Wall Interactions. submitted for publication.

KOUMOUTSAKOS, P., LEONARD, A & PEPIN, F. 1994 Boundary conditions for viscous vortex methods J. of Comput. Phys. 113, 52.

Le, H., Moin, P. & Kim, J 1997 Direct numerical simulation of turbulent flow over a backward-facing step. J. Fluid Mech. 330, 349-374.

Lee, C., Kim, J., Babcock, D., & Goodman, R. 1997 Application of neural network to turbulence control for drag reduction. Phys. Fluids A9, 1740-1747.

LIGHTHILL, M.J. 1963 Introduction. Boundary Layer Theory. J. Rosenhead (editor) - Oxford Univeristy PressNew York, 54-61 LÖFDAHL, L., KÄLVESTEN, E., & STEMME, G. 1996 Small silicon pressure transducers for space-time correlation measurements in a flat plate boundary layer J. of Fluids Engin. 118, 457-463.

Moin, P., & Bewley, T.R. 1995 Application of control theory to turbulence Twelfth Australasian Fluid Mechanics Conference, Dec. 10-15, Sydney, 109-117.

ORLANDI, P. 1990 Vortex dipole rebound from a wall. Phys. Fluids A1429, 75-110.

Panton, R.L. 1984 Incompressible Flow. Wiley.

RECHENBERG, I. 1973 Evolutionsstrategie: Optimierung technischer System nach Prinzipien der biologischen Evolution Fromman-Holzboog, Stuttgart.

Schwefel, H.P. 1977 Numerische Optimierung von Computer-Modellen mittels der Evolutionsstrategie. Birkhäuser Verlag, Basel.

Wu, J.Z., Wu, X.H., & Wu, J.M. 1993 Streaming Vorticity Flux from Oscillating walls with finite amplitude. Phys. of Fluids A5, 1933-1938.